Physics-Based Modeling of Active and Passive Microwave Covariations Over Vegetated Surfaces

Thomas Jagdhuber, *Member, IEEE*, Alexandra G. Konings, *Member, IEEE*, Kaighin A. McColl, *Member, IEEE*, Seyed Hamed Alemohammad, *Member, IEEE*, Narendra Narayan Das, Carsten Montzka, *Member, IEEE*, Moritz Link, *Student Member, IEEE*, Ruzbeh Akbar, *Member, IEEE*, and Dara Entekhabi, *Fellow, IEEE*

***Abstract*— Active and passive low-frequency microwave measurements from a number of space- and airborne instruments are used to estimate soil moisture. Each of the sensing approaches has distinct advantages and disadvantages. There is increasing interest in combining active and passive measurements in order to realize the advantages and alleviate the disadvantages. In order to combine active and passive measurements, their covariations with respect to soil moisture need to be known. The covariation is dependent on how the active and passive microwaves interact with vegetation canopy and soil surface. In this paper, we introduce a physics-based model for the covariation of active and passive microwaves over soil surfaces with vegetation cover. The analytical form for a covariation function is derived which depends on the scattering and absorption of microwaves by soil and vegetation with different orientations, structures, and water contents. The main finding is that the covariation function β is related to the roughness and vegetation losses in the two measurements. An increase in soil roughness or in vegetation cover leads to less negative values of β, which is pronounced for dense and moist vegetation. Both the soil and vegetation components introduce a polarization dependence of β that is caused by polarization-induced differences in soil scattering and oriented plant structures. The forward modeled covariations are plotted together with statistically derived covariation estimates from two months of global active and passive L-band observations of the Soil Moisture Active Passive mission. The physically modeled and statistically derived estimates of covariation are comparable in magnitude and scale.**

***Index Terms*— Active–passive microwave sensing, radiometer, synthetic aperture radar (SAR), soil moisture, Soil Moisture Active Passive (SMAP), vegetation attenuation and scattering.**

I. Introduction

INFORMATION on soil moisture at global scale is needed to understand and to model global climate, weather, and hydrological processes as well as their impacts on society [1], [2]. Despite its small absolute amount compared to other water storages on earth, soil moisture exerts control on interactions within the water cycle (e.g., land–atmosphere) and links the water, energy, and carbon cycles [3]. In order to sense the land surface regardless of cloud cover and solar illumination, microwave bands are preferred over optical and thermal frequencies. Lower frequency microwave channels partially penetrate through closed vegetation cover [4]. They also have a deeper soil sensing depth [5].

However, the size of the antenna limits the spatial resolution of low-frequency passive microwave measurements from low-earth orbit. Active microwave measurements can achieve higher resolution through synthetic aperture radar (SAR) processing [6]. The vegetation cover and surface soil conditions affect both active and passive microwave signals [7]. The interactions are more complex in the case of the active signal because the sensitivity of radar backscatter to soil and vegetation depends on several parameters. These include soil roughness (typically characterized by root-mean-squared height, correlation length scale, and the choice for the correlation function) and vegetation structure (including geometry, distribution, and dielectric properties). There is also a tradeoff between resolution and soil moisture sensing sensitivity between active and passive microwave measurements [8]. Ideally, the two can be combined to extract the relative advantages of the two sensing approaches [9]. In order to combine active and passive low-frequency microwave measurements, the covariations of the two measurements in the presence of variations in soil moisture need to be known. The covariation is the fundamental building block of active–passive soil moisture retrieval algorithms. It is strongly dependent on combinations of microwave channels and acquisition geometries. Analysis of the covariation for rough but bare soil surfaces is feasible

Manuscript received January 12, 2017; revised October 27, 2017 and April 24, 2018; accepted July 9, 2018. This work was supported by the NASA Soil Moisture Active Passive Project and the MIT-Germany Seed Fund "Global Water Cycle and Environmental Monitoring using Active and Passive Satellite-based Microwave Instruments." Moreover, Prof. P. Ferrazzoli and the anonymous reviewers are greatly acknowledged for their perceptive comments and valuable recommendations. *(Corresponding author: Thomas Jagdhuber.)*

T. Jagdhuber is with the Microwaves and Radar Institute, German Aerospace Center, 82234 Weßling, Germany (e-mail: thomas.jagdhuber@dlr.de).

A. G. Konings is with the Department of Earth System Science, Stanford University, Standford, CA 94305 USA.

K. A. McColl is with the Department of Earth and Planetary Sciences, Harvard University, Cambridge, MA 02138 USA.

S. H. Alemohammad is with the Department of Earth and Environmental Engineering, Columbia University, New York, NY 10027 USA.

N. N. Das is with the Jet Propulsion Laboratory, California Institute of Technology, Pasadena, CA 91109 USA.

C. Montzka is with the Institute of Bio- and Geosciences: Agrosphere, Research Centre Jülich, 52428 Jülich, Germany.

M. Link is with the Department of Geography, Ludwig-Maximilians University Munich, 80333 Munich, Germany, and also with the Microwaves and Radar Institute, German Aerospace Center, Oberpfaffenhofen, Germany.

R. Akbar and D. Entekhabi are with the Department of Civil and Environmental Engineering, Massachusetts Institute of Technology, Cambridge, MA 02139 USA.

Color versions of one or more of the figures in this paper are available online at http://ieeexplore.ieee.org.

Digital Object Identifier 10.1109/TGRS.2018.2860630

using theoretical (numerical) models (see [5], [10]–[14]). Incorporating the influence of the vegetation cover is not as well understood. Recently, a number of cases have been explored using analytical and parameterized models [15]–[24].

In this paper, we propose a physics-based, analytical (closed-form) formulation for the covariation that is dependent on the specification of microwave wavelength and incidence angle combinations, on vegetation and its structure, and on the statistics of soil roughness. The physical forward model of covariation serves as a guide for the design of active–passive surface soil moisture retrieval algorithms. The radar and radiometer can be on the same airborne or space-borne platform, but it can also be applied to measurements which are made on different platforms. Combining active and passive microwave measurements from different platforms are an emerging opportunity. Currently, there are excellent active and passive microwave sensors (e.g., TanDEM-X, Sentinel-1A/B, RADARSAT-2, and ALOS-2 for the active, European Space Agency's Soil Moisture Ocean Salinity, Japan Aerospace Exploration Agency's Advanced Microwave Scanning Radiometer 2, and National Aeronautics and Space Administration's (NASA) Soil Moisture Active Passive (SMAP) missions for the passive) making routine and global environmental measurements on different platforms. The combination of the two measurement types in a unified active–passive algorithm is an emerging opportunity. The forward model of active–passive microwave covariations, introduced in this paper, is meant to enable the realization of these opportunities.

This physical covariation model provides insight into the role of vegetation and identifies limits to sensing under dense canopies and distinct soil roughness. It is compared to global active and passive L-band (1.2–1.4 [GHz]) space-borne observations. The observed covariability is based on time series of active and passive measurements from the SMAP mission. The SMAP mission uses a radiometer in combination with an SAR, operating with a shared L-band horn antenna and a deployable, spinning mesh reflector [9], [26]. The radiometer measures H- and V-polarized brightness temperatures (as well as the third and fourth Stokes parameters) with a relative accuracy of 1.1 [K], while the SAR acquires HH and VV copolarized backscatter and one cross-polarized (HV or VH) backscatter with a relative accuracy of 0.5 [dB] [9], [26]. The data are acquired at 40° fixed incidence angle (off-nadir) by a conical scan across a 1000 [km] swath and at a fixed local time (6 A.M.) [25]. The two instruments operate on different scales: SAR products are provided at 3 [km] while radiometer products are available at 36 [km] (based on -3 [dB] or half-power definition), respectively. Unfortunately, the SMAP radar only collected global data for 11 weeks (April 14, 2015–July 7, 2015) before it stopped transmitting due to an instrument anomaly. Nevertheless, the SMAP observations from this period comprise an unprecedented global-scale data set for studying covariation between active and passive microwaves and for preparing future combined active- and passive-based surface soil moisture products (e.g., SMAP L-band radiometer and Sentinel-1A/B C-band radar).

In course of the preparation for the SMAP mission, a variety of downscaling approaches were developed. For example, Bayesian merging [27], ensemble Kalman smoothing [28], or change detection [29], [30] was proposed and some tested on airborne campaign data [8], [31]–[34].

The SMAP active–passive approach to surface soil moisture estimation at an intermediate 9 [km] scale is to combine the sensitivity advantage of the brightness temperature for soil moisture with the resolution advantage of the SAR data [30], [31], [35]. For the operational active–passive product, the SMAP algorithm uses the fine-scale SAR backscattering coefficients to downscale the coarse-scale radiometer brightness temperatures to intermediate-scale ones, from which soil moisture is retrieved [8], [31], [36].

The current baseline algorithm of the SMAP active–passive product uses a statistical (time-series regression) approach to estimate the covariation between the coincident SAR backscattering coefficients and the radiometer brightness temperature measurements [8], [31], [36]. The statistically determined slope of this linear relationship–denoted β–represents the covariation and is determined by regressing over a time series of active–passive SMAP acquisitions. Therefore, it is assumed that there is a separation of time scales between surface moisture variations and changes in vegetation and surface roughness. Thus, over finite-time windows, only variations in soil moisture contribute to covariations in radar and radiometer observations. But for each time window, the strength of the relationship is dependent on the soil roughness and vegetation conditions. This statistical approach is sensitive to temporal variation in soil roughness and vegetation cover (e.g., changing soil conditions and different phenological stages of vegetation). Therefore, the regression needs to be updated for each location and performed over a moving subseasonal window in time. Previous studies have used data from airborne campaigns [30], [33], [36], [37] and the Aquarius satellite [38] to study covariation (β) using regression for different temporal windows. However, estimating the optimal temporal window is challenging: if the window is too short, the small sample size may lead to substantial error in the covariation estimate. If the window is too long, vegetation and soil conditions may change over the window and bias covariation estimates [34], [39], [40].

In this paper, a physical model for covariation (β) is introduced, which avoids challenges in statistically estimating β from time series, and provides insights into the expected behavior of the covariation under different soil and vegetation conditions. In Section II, a general, physics-based formulation for covariation is derived based on Kirchhoff's law of energy conservation. Subsequently, basic formulations of covariation parameter β for bare and vegetated soils are formulated. The variations of β for different soil and vegetation conditions are then examined in Section III. In addition, forward model estimates of covariation are compared to those obtained based on regression with SMAP data. Finally, Section IV provides the summary and conclusions.

II. Derivation of a Physical Model for Active–Passive Microwave Covariation

In this section, we first introduce the physical basis to link active and passive microwaves for bare soils (Section II-A).

Next, we describe the scattering (Section II-B) and emission (Section II-C) scenarios for vegetated surfaces. This is followed by the formulation of active and passive microwave models for vegetated surfaces. We introduce the concept of active–passive microwave covariation in Section II-D. Finally, we derive the general physical model for β and covariation of vegetated and bare soils (Section II-E).

A. Combination of Active and Passive Microwaves for Bare Soils

In order to link emissivities with reflectivities in the microwave domain, Kirchhoff's law of energy conservation is applied [41], [42, p. 252]. Under thermodynamic equilibrium conditions in a half-space environment Kirchhoff's law can be expressed as [18], [24], [42], [43]

$$\begin{aligned} E_P = \frac{Tb_P}{T} &= 1 - \frac{1}{4\pi\cos\theta_i}\int_{\phi_s=0}^{2\pi}\int_{\theta_s=0}^{\frac{\pi}{2}} \big(|S_{PP}|^2(\theta_i,\phi_i,\theta_s,\phi_s) \\ &\quad + |S_{PQ}|^2(\theta_i,\phi_i,\theta_s,\phi_s)\big)\sin\theta_s d\theta_s d\phi_s \\ &= 1 - (R^{\text{coh}} + R^{\text{inc}}). \end{aligned} \tag{1}$$

Equation (1) links the p-polarized emissivity E_P [−] to the bistatic scattering coefficient S_{PQ} including a coherent (specular) forward R^{coh} [−] and an incoherent (diffuse) R^{inc} [−] scattering component of the soil surface [10], [13], [41], [42]. Here, Tb_P [K] is the p-polarized brightness temperature and T [K] is the effective physical temperature. The local incidence and scattering angles are θ_i [rad] and θ_s [rad], and ϕ_i [rad] and ϕ_s [rad] are the incident and scattered azimuthal angles.

Hereafter, the general concept of (1) is refined for long-wavelength (L-band) scattering over minor rough, nonvegetated soils. Roughness strongly affects the magnitude of emission. Surface roughness is characterized by its vertical component ks [−], the wavelength-scaled root-mean-square height of the surface [5]. At L-band and typically when ks $\leq$ 0.3 or s around 1 cm, incoherent emission becomes minor ($R^{\text{inc}} \to 0$) and the coherent (specular) term dominates scattering reducing (1) to [5, p. 825f], [44], [45]

$$E_P = 1 - R^{\text{coh}}. \tag{2}$$

The coherent surface reflectivity R^{coh} [−] is taken to be Fresnel R_P^F, with $R_H^F = |(\cos\theta_i - (\varepsilon_s - \sin^2\theta_i)^{1/2}/\cos\theta_i + (\varepsilon_s - \sin^2\theta_i)^{1/2})|^2$[−], $R_V^F = |(\varepsilon_s \times \cos\theta_i - (\varepsilon_s - \sin^2\theta_i)^{1/2}/\varepsilon_s \times \cos\theta_i + (\varepsilon_s - \sin^2\theta_i)^{1/2})|^2$ [−], where ε_s [–] is the soil dielectric constant. Together with the Fresnel surface roughness loss $f_F = e^{-4\times k^2\times s^2\times\cos^2\theta_i}$ [−] (2) may be written as [5], [42]

$$E_P = 1 - f_F \times R_P^F. \tag{3}$$

At L-band (with a wavelength of about 23 [cm]), the soil roughness is about one order of magnitude smaller than the wavelength with root-mean-square heights between 0.5 and 1 cm [46], [47]. The SAR reflection and scattering interactions with the surface can therefore be described by the small perturbation model, also called the Bragg model, applicable for smooth to moderately rough surfaces (ks $\leq$ 0.3) [5]. Hence, the measured copolarized surface backscatter $|S_{PP}|^2$ [−] for the active SAR scattering component is modeled as

$$|S_{PP}|^2 = f_B \times R_P^B \tag{4}$$

where f_B is the combined Bragg scattering and loss term (assuming an exponential spatial correlation function) $f_B = 8 \times (\cos^2\theta_i \times k \times s \times k \times l)^2 \cdot (1 + (2 \times k \times l \times \sin\theta_i)^2)^{-(3/2)}$ [−] [5], [42], [48]. The term $k \times l$ [−] is the wavelength-scaled autocorrelation length (horizontal component of soil surface roughness) and R_P^B [−] is the smooth Bragg surface reflectivity, $R_H^B = R_H^F$ and $R_V^B = |((\varepsilon_s - 1)(\sin^2\theta_i - \varepsilon_s \times (1 + \sin^2\theta_i))/(\varepsilon_s \times \cos\theta_i + (\varepsilon_s - \sin^2\theta_i)^{1/2})^2)|^2$ [–] [5], [10].

In order to link passive (3) and active (4) microwaves, the equivalence of scattering coefficients will be used. Therefore, Bragg reflectivity (R_P^B) in (4) needs to be expressed as proportional to the Fresnel reflectivity (R_P^F), present in (3), by dividing and multiplying (4) with R_P^F. This results in

$$|S_{PP}|^2 = f_B \times \kappa \times R_P^F \tag{5}$$

with conversion coefficient $\kappa = (R_P^B / R_P^F)$ [−]. Thus, Fresnel surface reflectivity R_P^F is the link to combine active and passive microwaves via energy conservation. Finally, solving for R_P^F in (5) and substituting this into (3) establishes the link between the emissivity and the backscatter

$$E_P = 1 - f_F \times R_P^F = 1 - \frac{f_F}{f_B \times \kappa}|S_{PP}|^2 \tag{6}$$

which is valid for smooth and moderately rough bare surfaces. This concept of connecting active and passive microwaves will also apply for vegetated soils in Section II-D, but first the scattering (Section II-B) and emission (Section II-C) scenarios for the vegetated soil case are introduced.

B. Microwave Scattering in Case of Vegetation Covered Surfaces

Radar scattering in the presence of vegetated soils can be formulated based on the first-order distorted Born approximation as [49]–[51]

$$|S_{PP}|^2 = f_B \times \left|S_{PP}^B\right|^2 + f_D \times \left|S_{PP}^D\right|^2 + f_V \times \left|S_{PP}^V\right|^2. \tag{7}$$

Equation (7) is composed of a surface contribution $f_B|S_{PP}^B|^2$ [−], a (double-bounce) surface-vegetation interaction contribution $f_D|S_{PP}^D|^2$ [−] and a direct vegetation volume contribution $f_V|S_{PP}^V|^2$ [−]. The terms f_B [−], f_D [−], and f_V [−] are the scattering and loss terms for the surface, double-bounce, and volume scattering contribution, respectively. A variety of empirical, semiempirical, and theoretical scattering models exist for the variables in (7). Empirical and semiempirical models are based on experimental data that are limited to the vegetation structure of the case study. Theoretical results are available for models of vegetation as collection of lossy dielectric shapes such as cylinders for trunks and branches and discs for leaves [5], [7], [49], [52]. We adopt the latter approach for vegetation and can describe it as a continuous or discrete medium (see [53], [54]). The discrete approach is suitable for covariation modeling because it allows

simulation of the backscatter from an ensemble of discrete objects with diverse physical properties (see [55], [56]). One parsimonious and effective approach, using a homogeneously filled layer of lossy dielectric discs (plant elements) above a single-scattering nonpenetrable soil surface, is proposed by Lang and Sidu [51] and Lang [57]. This approach is implemented to express the variables of (7) in terms of surface, double-bounce, and volume reflection terms and to parameterize soil scattering for connecting active and passive microwaves. The surface $f_B \times |S^B_{PP}|^2$ and double $f_D \times |S^D_{PP}|^2$ bounce terms describe incoherent and coherent interactions with the soil surface, which can be expressed by rough Fresnel surface reflection $f_F \times R^F_P$, when applying (5) for the incoherent interactions. Surface reflectivity R^F_P will be used to connect the active and passive microwave domains in Section II-D.

Following Lang and Sidu [51], the surface and double-bounce terms are defined as function of R^F_P:

$$f_B \times \left|S^B_{PP}\right|^2 = f_B \times \gamma^2_{R_P} \times R^B_P = f_B \times \kappa \times \gamma^2_{R_P} \times R^F_P \quad (8)$$

$$f_D \times |S^D_{PP}|^2 = \frac{k^4 \times \delta \times V_D \times d}{4\pi} 4 \times \overline{|a_{PP}|^2} \times f_F \times \gamma^2_{R_P} \times R^F_P \quad (9)$$

where $\overline{|a_{PP}|^2}$ [−] is the mean squared polarizability of the vegetation bounce in the double-bounce term [57]. Variable d [m] is the height of the vegetation layer. Wavenumber k [m^{-1}] is ($k = 2\pi/\lambda$) where λ [m] denotes the wavelength of the system. Variable $\delta = \rho \times V_D$ [−] is the fractional volume of the vegetation defined by the particle density $\rho = N/V$ [m^{-3}] (number of vegetation inclusions N divided by total volume V [m^3]) and the volume of the single vegetation disk element V_D [m^3]. Here, V_D is defined in terms of the radius a [m] and the thickness h [m] of the single element as $V_D = \pi \times a^2 \times h$. A two-way vegetation attenuation $\gamma^2_{R_P}$ through the vegetation applies to the direct surface and the double-bounce contribution and it is defined after Lang and Sidu [51] as $\gamma^2_{R_P} = |e^{2\times i \times k_{zP} \times d}|^2$ [−], where $k_{zP} = k \times \cos\theta_i + k^2 \times a_{pp} \times \delta/(2 \times k \times \cos\theta_i)$ [m^{-1}] is the polarization-dependent propagation term.

By substituting (8) and (9) into (7), the total SAR backscatter is

$$|S_{PP}|^2 = f_B \times \kappa \times \gamma^2_{R_P} \times R^F_P + \frac{k^4 \times \delta \times V_D \times d}{\pi} \overline{|a_{PP}|^2} \times f_F \times \gamma^2_{R_P} \times R^F_P + f_V \times \left|S^V_{PP}\right|^2. \quad (10)$$

Both ground scattering contributions (surface and double bounce) are now a function of the Fresnel reflectivity R^F_P which will connect the active and passive domains in Section II-D.

C. Microwave Emission in Case of Vegetation-Covered Surfaces

In the presence of vegetation, microwave emission relation to soil and vegetation physical conditions can be approximated using the zeroth-order solution of the radiative transfer equation or the $\tau - \omega$ model [5], [7], [58]. It captures three contributions: direct emission from vegetation Tb_V, soil-reflected emission from vegetation Tb_{VS}, and direct emission from soil Tb_S. As emissions with soil contribution (Tb_S, Tb_{VS}) can also be related inversely to lossy Fresnel reflectivity $f_F \times R^F_P$, used later as link for active-passive microwave combination, the $\tau - \omega$ model can be written as [59]

$$Tb_P = Tb_V + Tb_{VS} + Tb_S = T_V \times (1-\omega)(1-\gamma) \times \left(1 + f_F \times R^F_P \times \gamma\right) + T_S \times \left(1 - f_F \times R^F_P\right) \times \gamma \quad (11)$$

where $\gamma = e^{-\tau/\cos\theta_i}$ [−] is the one-way vegetation loss term and considered to be the same for both polarizations within the $\tau - \omega$ model [60]. θ_i [rad] is the incidence angle. The nadir vegetation opacity τ [−] is related empirically to the physical characteristics of the vegetation layer through $\tau = b \times \mathrm{VWC}$, where VWC [$\mathrm{kg/m}^2$] is the vegetation water content and b [m^2/kg] is a structure-dependent empirical parameter for the microwave opacity [55], [56], [58]. Variable ω [−] is the effective single scattering albedo. Both τ and ω are retrievable from radiometer data using a multitemporal, dual-channel estimation algorithm [61] or can be derived from other ancillary data [36], [59], [62]. Under the assumption of isothermal conditions ($T_S = T_V$) during SMAP acquisitions at 6 A.M. local time (11) is rewritten as [36]

$$\frac{Tb_P}{T} = E_P = (\gamma \times (1-\omega)(1-\gamma) - \gamma) \times f_F \times R^F_P + (\gamma + (1-\omega)(1-\gamma)) \quad (12)$$

whereby all emissions involving soil interaction are now a function of the Fresnel reflectivity R^F_P.

D. Combination of Active and Passive Microwaves for Vegetated Surfaces and Definition of Covariation Parameter β

Combining active and passive microwave terms is done via Fresnel reflectivity R^F_P, as shown for the bare soil case in Section II-A. The same principle applies for vegetated soils. In order to combine active and passive microwave terms (10) is solved for R^F_P

$$R^F_P = \frac{|S_{PP}|^2 - f_V \times \left|S^V_{PP}\right|^2}{f_B \times \kappa \times \gamma^2_{R_P} + \frac{k^4 \times \delta \times V_D \times d}{4\pi} 4 \times \overline{|a_{PP}|^2} \times f_F \times \gamma^2_{R_P}}. \quad (13)$$

Substituting (13) in (12) and applying some rearrangement results in

$$E_P = \frac{f_F \times (\gamma(1-\omega)(1-\gamma) - \gamma)}{f_B \times \kappa \times \gamma^2_{R_P} + f_F \times \gamma^2_{R_P} \times V_D \times k^4 \frac{d \times \delta}{\pi} \overline{|a_{pp}|^2}} \times \left(|S_{PP}|^2 - f_V \times \left|S^V_{PP}\right|^2\right) + \gamma + (1-\omega)(1-\gamma). \quad (14)$$

Equation (14) is a linear physics-based relationship linking the total backscattering coefficient $|S_{PP}|^2$ measured by the SAR and the emissivity E_P observed by the radiometer. This linear formulation is identical in form to the SMAP baseline active-passive disaggregation model described in (10) of [36], which was established empirically in prestudies to the mission [31]–[34]. In this statistical approach the SAR backscatter intensity $|S_{PP}|^2$ is related linearly to the emission

measured with the radiometer E_P by the slope β_{p-pp} [−] and the intercept α_{p-pp} [−] of the time-series linear regression

$$E_P = \beta_{p-pp} \times |S_{PP}|^2 + \alpha_{p-pp}. \quad (15)$$

The physics-based model for the covariation of emission and backscatter in (14) demonstrates the linearity of the active–passive microwave covariation which results in the expressions of the β_{p-pp} and α_{p-pp} parameters in (15)

$$\beta_{p-pp} = \frac{f_{F\times}(\gamma(1-\omega)(1-\gamma)-\gamma)}{f_B \times \kappa \times \gamma_{R_P}^2 + f_F \times \gamma_{R_P}^2 \times V_D \times k^4 \frac{d\times\delta}{\pi} \overline{|a_{pp}|^2}} \quad (16)$$

and

$$\alpha_{p-pp} = -\frac{f_F \times (\gamma(1-\omega)(1-\gamma)-\gamma)}{f_B \times \kappa \times \gamma_{R_P}^2 + f_F \times \gamma_{R_P}^2 \times V_D \times k^4 \frac{d\times\delta}{\pi} \overline{|a_{pp}|^2}} \times f_V \times |S_{PP}^V|^2 + (\gamma + (1-\omega)(1-\gamma)). \quad (17)$$

The volume-only scattering ($f_V \times |S_{PP}^V|^2$) and volume-only emission ($\gamma + (1-\omega)(1-\gamma)$) components appear separately and can only be found in α_{p-pp}. Therefore, β_{p-pp} is independent of both direct vegetation volume emission as well as scattering. The active-passive disaggregation approach used in the SMAP algorithm does not require estimates of α_{p-pp}, but it is strongly influenced by the parameter β_{p-pp} [36], which is modeled on physics basis in the following.

E. Physical Model of Covariation for Vegetated and Bare Soils

The physical model of emission and backscatter covariations with respect to surface dielectric constant (soil moisture) changes are dependent on polarization, dielectric and structural characteristics of vegetation, and roughness of the soil surface. Using (16), they can be summarized as

$$\beta_{\text{Veg}}^{h-hh} = \frac{f_F \times (\gamma(1-\omega)(1-\gamma)-\gamma)}{f_B \times \kappa \times \gamma_{R_H}^2 + f_F \times \gamma_{R_H}^2 \times V_D \times k^4 \frac{d\times\delta}{\pi} \overline{|a_{HH}|^2}}$$
$$\beta_{\text{Veg}}^{v-vv} = \frac{f_F \times (\gamma(1-\omega)(1-\gamma)-\gamma)}{f_B \times \kappa \times \gamma_{R_V}^2 + f_F \times \gamma_{R_V}^2 \times V_D \times k^4 \frac{d\times\delta}{\pi} \overline{|a_{VV}|^2}}. \quad (18)$$

The expressions for the mean squared polarizabilities $\overline{|a_{HH}|^2}$ and $\overline{|a_{VV}|^2}$ as a function of vegetation layer characteristics are summarized in Appendix. The specification of the polarizabilities allows modeling $\beta_{\text{Veg}}^{p-pp}$ for vegetation structure of horizontally as well as vertically oriented canopies. The vegetation layer and the rough soil cause losses and scattering of the active and passive microwaves. A main insight derived from the expressions in (18) is that the covariation parameter $\beta_{\text{Veg}}^{p-pp}$ is the ratio emission losses divided by backscatter losses. The emission loss factors related to soil and vegetation (f_F, γ, ω) are evident in the numerator. The denominator includes the surface contribution backscatter loss factors ($f_B, \kappa, \gamma_{R_P}$) and the double bounce backscatter and loss factors (related to f_F, $\gamma_{R_P}, V_D, k, d, \delta, \overline{|a_{PP}|^2}$).

When only soil scattering is present (no vegetation cover such that $\gamma = 1$, $\omega = 0$, and $d = V_D = \delta = 0$), the covariation parameter in (18) reduces to $\beta_{\text{Bare}}^{p-pp}$

$$\beta_{\text{Bare}}^{p-pp} = -\frac{f_F}{f_B \times \kappa} = -\frac{f_F}{f_B \times \frac{R_P^B}{R_P^F}} \quad (19)$$

which is simply a combination of (3) and (5). The bare soil $\beta_{\text{Bare}}^{p-pp}$ is thus the ratio of Fresnel f_F and Bragg f_B roughness loss terms, scaled by κ. Soil roughness is the only physical variable controlling $\beta_{\text{Bare}}^{p-pp}$. For horizontal polarization $\beta_{\text{Bare}}^{h-hh} = -(f_F/f_B)$ because $\kappa = 1$ (identity of the Fresnel and Bragg reflectivity, $R_H^F = R_H^B$). For vertical polarization $\beta_{\text{Bare}}^{v-vv} = -(f_F/f_B \times \kappa)$ because $\kappa \neq 1$ and reflection coefficients differ ($R_V^F \neq R_V^B$). Section II-A introduced the expressions for the Bragg and Fresnel reflectivity and roughness losses

III. Analysis of the Physical Model for Covariation and Comparison With SMAP Estimates

In this section, we analyze the dependence and magnitude of the scattering and losses in SAR and radiometer expressed in (18) and (19) with respect to the physical roughness conditions of surface (parameters s and l) and vegetation (parameters d, δ, ω, and τ). We start with the simpler covariation scenario for bare soils and follow with the more complex vegetated surfaces. We investigate the sensitivity of the physical forward model for covariation to various surface roughness and vegetation characteristics in order to understand the dynamic range and behavior of active–passive microwave measurements in the context of soil moisture estimation. Covariation (β) can be either expressed as a dimensionless quantity [-] or in inverse decibels [dB^{-1}] depending on the units of $|S_{PP}|^2$ and values have previously been reported using both of these conventions [20], [30], [36], [38]. In the following sensitivity analysis, $|S_{PP}|^2$ is considered in linear units [directly relating to the underlying physics in (1)], so that covariation (β) is dimensionless. For system settings a constant $\theta_i = 40°$, incidence angle is assumed for both instruments and the frequency is fixed at L-band (SAR: 1.26 [GHz] and Radiometer: 1.41 [GHz]) identical to the original SMAP acquisition scenario (before failure of the SAR).

We first analyze the covariation scenarios for bare soils using the following soil conditions: the surface roughness is set to a low to medium roughness range with vertical and horizontal roughness statistics (s, l) of 0.005 [m] and 0.05 [m], respectively [46], [47]. The soil half-space medium is assumed to nominally have a mid-range moisture level represented by a dielectric constant $\varepsilon_S = 20 + 3i$ [63]. In the bare soil case, it is possible to compare the physical model $\beta_{\text{Bare}}^{p-pp}$ from (19) to independent sources of information: the integral equation method (IEM) and the 3-D numerical method of Maxwell's equations (NMM3D) model [10], [24], [64]. The NMM3D is a set of simulations based on numerical solutions of the Maxwell equations in 3-D. It is a rigorous source of numerical solutions data on bare but rough surface emissions and scattering. In addition, the well-known and frequently applied IEM is included as another physics-based model for comparison against the physics-based $\beta_{\text{Bare}}^{p-pp}$ forward model [64].

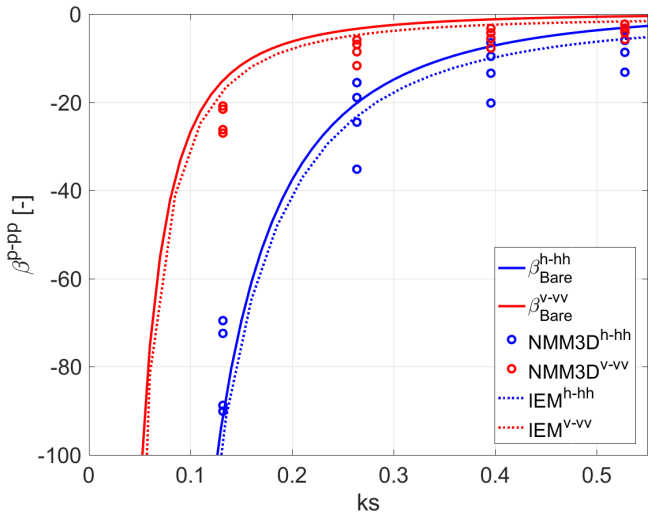

Fig. 1. Vertically (red lines) and horizontally (blue lines) polarized covariation parameter $\beta^{p-pp}_{\text{Bare}}$ from (19) or the forward model (solid lines) versus effective vertical roughness (ks) compared with statistically derived $\beta^{p-pp}_{\text{Bare}}$ values from NMM3D (circles) and IEM (dotted lines) model outputs. The *kl* value is 1.5 for the forward model and IEM. The NMM3D model is calculated for a range of four different *kl* values per *ks* value (see Table I).

TABLE I
SOIL ROUGHNESS VALUES FOR BARE SOIL SIMULATIONS WITH NMM3D

ks	0.13194689	0.26389378	0.39584067	0.52778757
kl	0.52778757	1.05557513	1.5833627	2.11115026
	0.92362824	1.84725648	2.77088472	3.69451296
	1.31946891	2.63893783	3.95840674	5.27787566
	1.97920337	3.95840674	5.93761012	7.91681349

Fig. 1 shows the vertical and horizontal polarizations of $\beta^{p-pp}_{\text{Bare}}$ for the three models (assuming 1.4 [GHz] emission and backscatter for easier comparison) along increasing soil roughness (*ks*) with a fixed correlation length (*kl*) of 1.5 for the forward model and IEM and a variable kl (see Table I) for NMM3D. The latter is considered as reference method and is therefore shown for varying both ks and kl.

In the cases of IEM (dashed lines) and NMM3D (symbols), the covariation parameter ($\beta^{p-pp}_{\text{Bare}}$) is calculated for each ks step as the statistical correlation between variations in emission and changes in backscatter within a range of potentially occurring soil dielectric constant values in nature. The solid lines in Fig. 1 are from (19) and represent the ratio of surface roughness-induced losses in the observed emission and backscatter. Generally, $\beta^{p-pp}_{\text{Bare}}$ decreases to less negative values with increasing roughness indicating a higher dynamic range of backscatter when compared to emissivity. Bare soil $\beta^{v-vv}_{\text{Bare}}$ decreases faster in magnitude than $\beta^{h-hh}_{\text{Bare}}$ due to different loss and scattering types (Fresnel, Bragg) in the ratio of (19). But for both, an upper and strictly negative bound for the covariation (β) can be found as characteristic of the physical model. This is consistent with statistically modeled (strictly negative) covariation in Guerriero *et al.* [20]. Although positive β-estimates are sometimes found for data-derived covariations, these are attributed to measurement uncertainties [31], [32], [36], [38].

Comparison can be made between the physical model (19) or $\beta^{p-pp}_{\text{Bare}}$ with the NMM3D retrievals as well as IEM retrievals of β^{p-pp}. All three β-estimates follow a sharp rise in magnitude with increase of roughness *ks*. Although with some offset, the three estimates for bare soil are consistent, but non-overlapping. The forward model marks the upper bound and NMM3D is near the lower bound of the value range.

These multicomponent polarimetric scattering models (IEM, NMM3D) at L-band are not fully captured by the parsimonious Fresnel and Bragg models implemented in the forward case. This explains the differences between the model simulations. The Fresnel and Bragg models represent two scattering types lacking the generality (large validity range for roughness) inherent to NMM3D or IEM. However, the Fresnel and Bragg scattering models are analytically tractable and computationally less intensive than NMM3D or IEM.

The transition of the scattering and emission scenario from bare to vegetated soil conditions increases the complexity of the forward model for covariation. The following behaviors of covariation parameter $\beta^{p-pp}_{\text{Veg}}$ are expected and tested using the forward model.

1) Also under vegetated soil conditions, $\beta^{p-pp}_{\text{Veg}}$ should increase toward zero with rising soil surface roughness (s, l) due to the higher roughness sensitivity of backscatter (SAR) in comparison with emissivity (radiometer).
2) $\beta^{p-pp}_{\text{Veg}}$ should increase toward less negative values with growing vegetation height d, vegetation fractional volume δ as well as VWC, as the backscatter sensitivity (SAR) is preserved mainly due to the effects of double bounce [20], while attenuation losses reduce emissivity dynamics (radiometer).

We test these hypotheses quantitatively by applying the developed physical model of covariation $\beta^{p-pp}_{\text{Veg}}$ in (18). The covariation model contains several vegetation parameters, so that the full parameter space cannot be explored explicitly. Instead, we combine parameters into physically meaningful groupings [for example, VWC as shown in (20)] and consider a nominal set of parameters that are chosen to be representative of a typical (agricultural) canopy. They are listed in Table II.

The vegetation volume is filled with lossy dielectric plant disc elements forming a volume of biomass. The physical density of the biomass ρ_E is to be compared with the liquid water ($\rho_W = 1000$ [kg/m^3]) and the nominal value is typical for a cropped stand of mature corn. Natural vegetation can have biomass physical density ρ_E as low as 100 [kg/m^3] depending on biome and type. The real part of the dielectric constant of the plants ε'_V is taken to be the gravimetric content that is water (physical density of biomass ρ_E divided by the density of water ρ_W) multiplied by the dielectric constant of water ($\varepsilon_W = 80{+}0i$) [65], [66]. The dielectric constant of vegetation is therefore retrieved effectively by $\varepsilon'_V = (\rho_E/\rho_W) \times \varepsilon_W$ (including $\varepsilon''_V = \varepsilon'_V/25$). This results in $\varepsilon_V = 57.7 + 2.3i$ as shown in Table II. Several of the vegetation parameters can

TABLE II
NOMINAL VALUES FOR SYSTEM, SOIL, AND VEGETATION VARIABLES

Variable	Symbol	Value	Unit
System			
Local incidence angle	θ_i	40	[Degree]
Radar wavelength (L-band)		0.238	[m]
Radiometer wavelength (L-band)		0.213	[m]
*Soil**			
Vertical roughness	s	0.005	[m]
Horizontal roughness	l	0. 05	[m]
Dielectric constant of soil	$\varepsilon_S^{'}, \varepsilon_S^{''}$	20+3i	[-]
*Vegetation**			
Dielectric constant of plant elements	$\varepsilon_V^{'}, \varepsilon_V^{''}$	57.7+2.3i	[-]
Physical density of plant elements	ρ_E	721	[kg/m³]
Radius of plant elements	a	0.05	[m]
Thickness of plant elements	h	0.0003	[m]
Orientation distribution width of plant elements	Δ	10	[Degree]
Density of canopy in plant elements/m³	ρ	400	[Count/m³]
Scattering albedo of canopy	ω	0.05	[-]
Microwave opacity parameter	b	0.11	[m²/kg]

* Soil and vegetation parameters refer to [46], [47] and [51.]

be combined to form the VWC [kg/m^2]

$$\mathrm{VWC} = \rho_E \times \rho \times V_D \times d = \rho_E \times \delta \times d. \qquad (20)$$

The VWC forms a useful combined parameter to represent the vegetation condition, and it will be used in Figs. 2–8 as the axis for vegetation.

In addition, the plant elements are strongly vertically oriented with a uniform and narrow (10°) plant orientation distribution width Δ with respect to the z-axis perpendicular to soil plane [51].

For emission, the scattering albedo and opacity of the covering vegetation are set to $\omega = 0.05$ and $b = 0.11$ (used in conjunction with VWC to estimate τ: see Section II-C) assuming a polarization-independent, vegetation attenuation of an average (agricultural) canopy [36], [58], [59], [62].

The model of $\beta_{\mathrm{Veg}}^{p-pp}$ allows polarization dependence due to preferential orientations within the vegetation volume leading to anisotropic scattering (SAR). Fig. 2 depicts $\beta_{\mathrm{Veg}}^{p-pp}$ for two orientation cases of the vegetation canopy with a plant orientation distribution width of 10° around the dominant polarization axis (see Table II). They result from the main orientation of the lossy dielectric elements (plant constituents) forming the volume. The top panel assumes dominant vertically oriented vegetation for $\beta_{\mathrm{Veg}}^{p-pp}$–modeling, whereby polarizabilities (α_{HH}, α_{VV}) are interchanged compared to (18), while the bottom panel describes a dominant horizontal one. The $\beta_{\mathrm{Veg}}^{p-pp}$ behavior of these two cases shows similar trends, but with interchanged polarizations caused by rotation of the reference frame. Due to these similar trends, we only consider the vertically oriented case in remaining analysis.

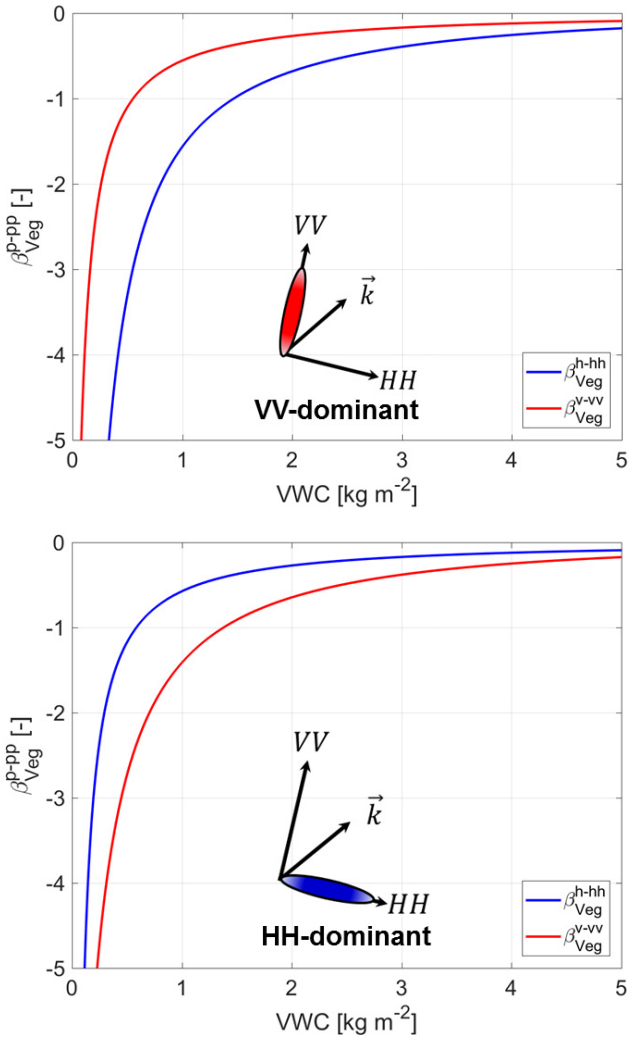

Fig. 2. Vertically (red lines) and horizontally (blue lines) polarized covariation parameter $\beta_{\mathrm{Veg}}^{p-pp}$ versus VWC [kg/m^2] for different main orientations of the vegetation canopy: (Top) vertically and (Bottom) horizontally oriented canopy.

$\beta_{\mathrm{Veg}}^{p-pp}$ is considerably smaller in magnitude when compared to $\beta_{\mathrm{Bare}}^{p-pp}$, under the same (nominal) roughness conditions (see Table II), due to significant amount of losses in the vegetation layer. It increases toward less negative values with rising VWC due to growing or wetting of the vegetation canopy. This confirms both hypotheses outlined earlier and is also consistent with simulated results from the TorVergata model [20]. Moreover, this behavior of covariation is also found in β-estimates from experimental and airborne campaigns ([30, Fig. 8]; [31, Fig. 4]; [32, Fig. 4]; [33, Fig. 5]; [36, Figs. 6 and 10]; [37, Fig. 5(b)]).

Even under vegetated canopies, the roughness of the soil is a factor in covariations of emission and backscatter, Fig. 3 shows the covariation parameter for vegetated soils $\beta_{\mathrm{Veg}}^{p-pp}$ versus VWC for different soil roughness (s) cases. Lower VWC results in larger spread in $\beta_{\mathrm{Veg}}^{p-pp}$ for different s-values. The same can be stated to a smaller extent for the horizontal component of the soil surface roughness l depicted in Fig. 4. For a VWC of about 0.1 [kg/m^2] or lower

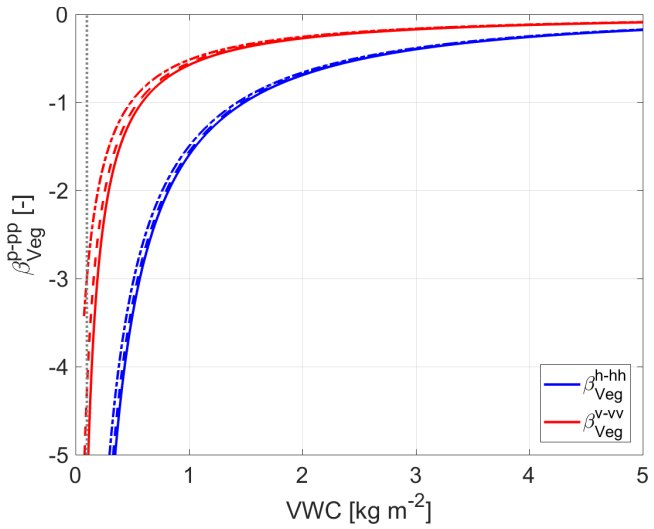

Fig. 3. Vertically (red lines) and horizontally (blue lines) polarized covariation parameter $\beta_{\text{Veg}}^{p-pp}$ as a function of increasing vegetation cover (VWC) for different vertical soil roughness values (s) [m]: solid line: $s = 0.0025$, dashed line: $s = 0.005$, dashed-dotted line: $s = 0.0075$; dotted vertical line indicates VWC value of 0.1 [kg/m^2].

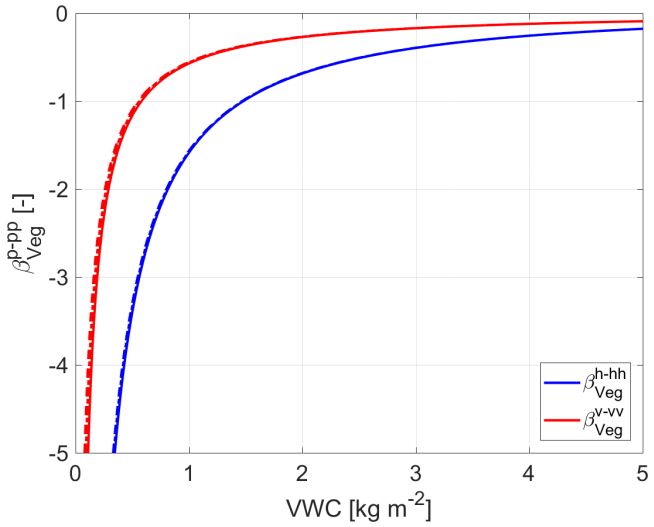

Fig. 4. Vertically (red lines) and horizontally (blue lines) polarized covariation parameter $\beta_{\text{Veg}}^{p-pp}$ as a function of increasing vegetation cover (VWC) for different horizontal soil roughness values (l) [m]: solid line: $l = 0.01$, dashed line: $l = 0.05$, and dashed-dotted line: $l = 0.09$.

(dotted line in Fig. 4), a pronounced change from slightly rough soils ($s = 0.0025$ [m]) to rough soils ($s = 0.0075$ [m]) is evident.

The absolute magnitude of $\beta_{\text{Veg}}^{p-pp}$ increases for vertical polarization toward less negative values from -5 to -3.

However, the magnitude level of $\beta_{\text{Veg}}^{p-pp}$ is still lower than for $\beta_{\text{Bare}}^{p-pp}$ due to the attenuating influence of vegetation cover. The asymptote of the covariation parameter toward zero is due to an increase in backscatter dynamic range mostly due to the effects of double-bounce (soil vegetation) scattering and a decrease of emissivity dynamic range due to vegetation attenuation.

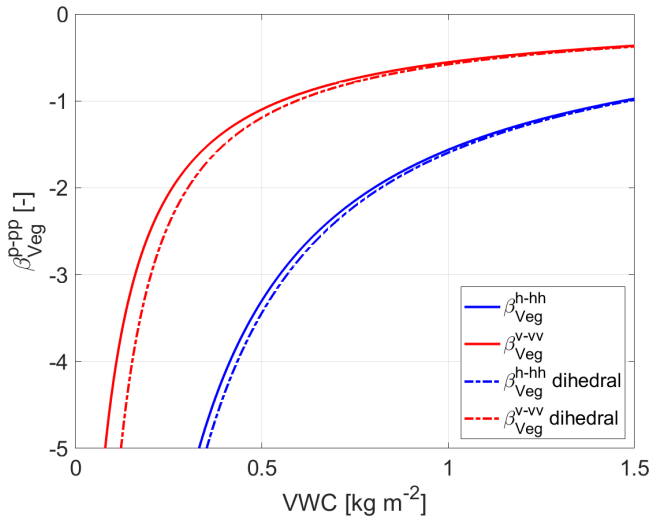

Fig. 5. $\beta_{\text{Veg}}^{p-pp}$ as a function of increasing vegetation cover (VWC) when both attenuated surface and double-bounce contributions are included (solid lines) and when only the double-bounce contribution is included (dashed lines).

The relative contribution of attenuated direct surface backscatter and double bounce can be discerned from (18). Fig. 5 shows $\beta_{\text{Veg}}^{p-pp}$ as a function of increasing vegetation cover (VWC) when both the attenuated surface contribution [first term in denominator of (18)] and the double-bounce contribution [second term in (18)] are included (solid lines). When only the proportion of double-bounce (soil-vegetation) contribution is included, it is plotted as dashed lines for both polarization pairs. $\beta_{\text{Veg}}^{p-pp}$ for the attenuated surface contribution (with magnitudes of -14 to -10 for vertical and -85 to -41 for horizontal polarization) is not shown in Fig. 5 to preserve readability.

The proximity of the curves indicates that the double-bounce term dominates the backscatter covariation over almost the entire VWC range. Only for sparse vegetation cover (VWC $<$ 0.5 [kg/m^2]), the single-bounce (surface scattering) term gives a more substantial contribution to the covariation. Since the distorted born approximation is used within the covariation model, higher order (multiple) scattering terms are not included and they may reduce the dominance of the double bounce term. For higher values of VWC (VWC $>$ 1.5 [kg/m^2]), both $\beta_{\text{Veg}}^{h-hh}$ and $\beta_{\text{Veg}}^{v-vv}$ converge to values close to zero due to a strongly diminished emissivity dynamic range, implying a reduced covariation of SAR and radiometer measurements. So far the dependencies on different soil surface conditions under a vegetation canopy have been explored.

Next, we examine the sensitivity of covariation ($\beta_{\text{Veg}}^{p-pp}$) to various vegetation conditions. Key among the vegetation parameters is the physical density of the single plant elements ρ_E [kg/m^3]. The physical density can be a fraction of the liquid water density $\rho_W = 1000$ [kg/m^3] depending on the relative amount of water and cellulose and lignin in the plant fiber. Mature crops tend to have higher values (up to 800 [kg/m^3]), but natural vegetation can have physical densities as low as 100 [kg/m^3] depending on biome and type. Fig. 6 shows the

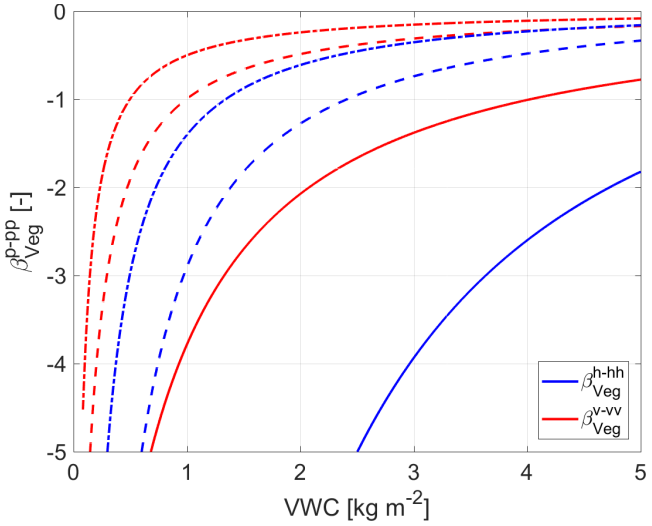

Fig. 6. Vertically (red lines) and horizontally (blue lines) polarized covariation parameter $\beta^{p-pp}_{\text{Veg}}$ for different physical plant densities (ρ_E) [kg/m^3] versus VWC [kg/m^2]: solid line: $\rho_E = 100$, dashed line: $\rho_E = 400$, and dashed-dotted line: $\rho_E = 800$.

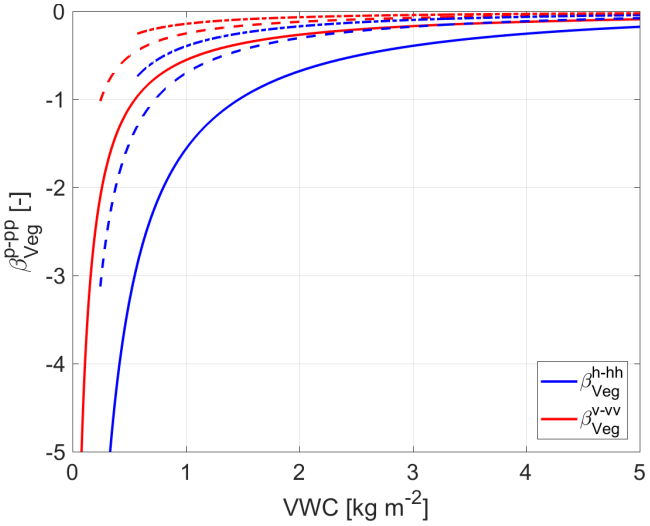

Fig. 7. Vertically (red lines) and horizontally (blue lines) polarized covariation parameter $\beta^{p-pp}_{\text{Veg}}$ for different leaf radii (a) [m] versus VWC [kg/m^2]: solid line: $a = 0.05$, dashed line: $a = 0.075$, and dashed-dotted line: $a = 0.1$.

behavior of $\beta^{p-pp}_{\text{Veg}}$ with respect to changes in the physical density of the single plant elements (ρ_E) forming the vegetation volume. The physical density is varied over a wide range of values. The covariation $\beta^{p-pp}_{\text{Veg}}$ decreases significantly in magnitude for vegetation with greater physical density. Both emission and backscatter attenuation are affected by the density. Furthermore, the vegetation bounce of the double-bounce contribution is affected (through the polarizability parameter).

Since a number of vegetation parameters are encapsulated in VWC [see Table II and related discussion surrounding estimation of VWC in (20)] and given that the covariation parameter is shown in the figures as a function of this grouped parameter, the sensitivity to the constituent parameters can be discerned from the dependence of $\beta^{p-pp}_{\text{Veg}}$ on VWC. Therefore, variations in factors, such as canopy density (ρ), radii and thickness of the plant elements (a^2 and h for $V_D = \pi a^2 h$), and vegetation height (d), generally follow the same effect on $\beta^{p-pp}_{\text{Veg}}$ as the one evident to VWC. The impact of variations in these encapsulated factors is expressed through respective variations in VWC. For the sake of parsimony, figures showing sensitivity to these parameters are generally not included.

The only exception is the radius of the plant elements (a), which is additionally displayed in Fig. 7 due to its square root dependence on $\beta^{p-pp}_{\text{Veg}}$. As a consequence, a significant decrease in $\beta^{p-pp}_{\text{Veg}}$ magnitudes is revealed with increasing plant radius.

Factors affecting emission also influence the dependence of $\beta^{p-pp}_{\text{Veg}}$ on VWC. Fig. 8 shows the sensitivity to the vegetation opacity parameter b. The influence of b on covariation ($\beta^{p-pp}_{\text{Veg}}$) directly correlates with the increase in VWC via $\tau = b \times \text{VWC}$ and is therefore negligible for sparse vegetation cover and more distinct at VWC levels of 0.7 [kg/m^2] and higher. The dynamic range of the numerator in (18) or emission is reduced with increasing values of b. Hence, higher

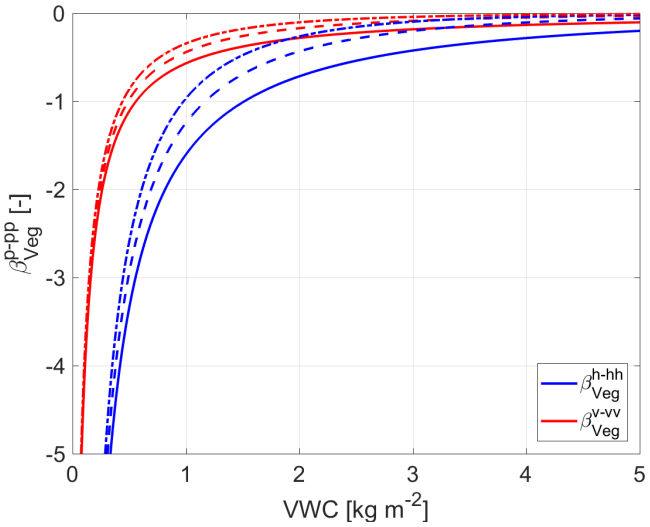

Fig. 8. Vertically (red) and horizontally (blue) polarized covariation parameter $\beta^{p-pp}_{\text{Veg}}$ for a different opacity parameter b [m^2/kg] versus VWC [kg/m^2]: solid line: $b = 0.1$, dashed line: $b = 0.2$, and dashed-dotted line: $b = 0.3$.

values of this parameter lead to reduced covariation between emission and backscatter for more dense canopies. From the structure of (18), it is evident that the other major emission parameter, namely, the scattering albedo ω also influences the dynamic range of emission. However, its influence on covariation is negligible ($\Delta\beta^{p-pp}_{\text{Veg}}$ <0.1) given the variation of its dynamic range from 0.02 to 0.12 (not shown).

In summary, the $\beta^{p-pp}_{\text{Veg}}$ relationships presented in Figs. 2–8 show the effects of surface roughness and VWC on the covariation between emission and backscatter. The covariation is with respect to changing soil dielectric constant (soil moisture) for a given vegetation cover depending on geographic location. Roughness affects both the emission and backscatter (direct surface and double-bounce) terms in the numerator and denominator of (18). Increasing

vegetation cover significantly reduces the dynamic range of both emission and backscatter and thus affects the covariation. The covariation amplitude is large for low-density vegetation, but eventually and with increasing vegetation cover, the amplitudes of the emission and backscatter are reduced and the surface soil conditions are no longer detectable.

The magnitude of the covariation parameter $\beta_{\text{Veg}}^{p-pp}$ can be compared with regression-based covariation estimates from field campaign and satellite-measured active–passive data sets [30], [31], [37], [38]. However, there are challenges in making direct comparisons between model and measurements.

First, high-quality field measurements of vegetation structure content (ρ and ρ_E) and VWC are typically not available in experimental field campaigns, especially not over the entire range of physically possible values. Estimates of VWC are often based on optical observations which observe only the canopy top and not the full vegetation volume. Recently, some studies use the radar vegetation index (RVI) as a proxy for VWC [67]–[69]. However, the relationship between RVI and VWC is error prone. For example, RVI may be biased by contributions from the ground signal depending on the penetration depth at L-band and would need to be removed by polarimetric decompositions [70], [71]. A second challenge is that field campaigns are usually short in duration which does not allow robust time-series regression for the covariation parameter β.

Konings *et al.* [61] developed a methodology to estimate vegetation opacity τ [−] from time series of L-band brightness temperature observations in two polarizations. Based on the application of the same methodology to SMAP measurements, a data set on τ is available for analysis. The opacity can be converted to estimates of VWC through the parameter b (see Table II). Furthermore, the global SMAP radar and radiometer colocated observations, introduced in [72] and ranging from April 14, 2015 to July 7, 2015 (period of available SMAP backscatter measurements), can be used to estimate $\beta_{\text{Veg}}^{p-pp}$ through time-series regression according to the SMAP active–passive baseline algorithm [36]. These two measurements-derived data sets provide an independent set of $\beta_{\text{Veg}}^{p-pp}$-VWC estimates that can be compared with the physics-based forward model developed in this paper. Figs. 9 and 10 show a comparison of the forward modeled covariation parameter $\beta_{\text{Veg}}^{p-pp}$ for horizontal and vertical polarizations, respectively. The color-shaded background shows the measurement-derived $\beta_{\text{SMAP}}^{p-pp}$-VWC estimates and the color shading is the frequency of occurrence of the pairs across the global land surface. The lines in Figs. 9 and 10 are based on (18) for the nominal parameters of Table II and for a range of plant physical densities (ρ_E). In order to keep consistency and comparability with former modeled results (see Figs. 2–8), the parameters of the forward model (lines) in Figs. 9 and 10 are not optimized for different regions on the globe. They remain as the nominal values in Table II except for physical plant density which is shown for its dynamic range. Hence, only the magnitude of the covariation parameter $\beta_{\text{Veg}}^{p-pp}$ and its trend with increasing VWC should be compared. The results in Figs. 9 and 10 show that the functional form

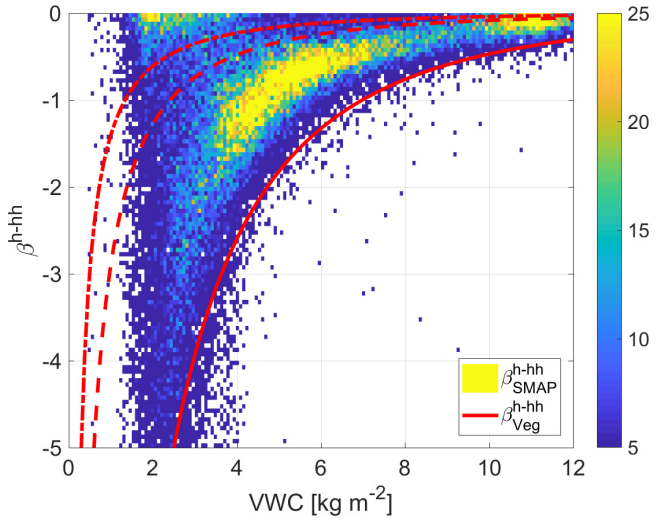

Fig. 9. Covariation parameter $\beta_{\text{Veg}}^{h-hh}$ modeled along VWC [kg/m^2] with different physical plant densities (ρ_E) [kg/m^3]: 100 (solid line), 400 (dashed line), 800 (dashed dotted line) on top of a bivariate (2-D) histogram of global, SMAP-derived $\beta_{\text{SMAP}}^{h-hh}$-values (excluding ice-covered regions); coloring of histogram from dark blue (low counts) to yellow (high counts).

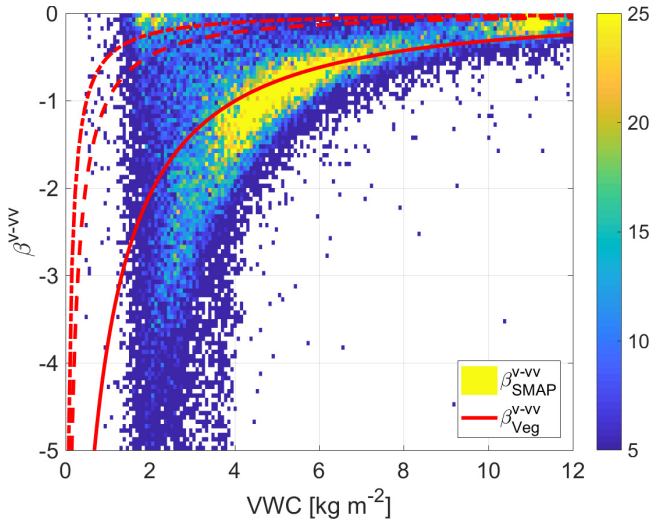

Fig. 10. Covariation parameter $\beta_{\text{Veg}}^{v-vv}$ modeled along VWC [kg/m^2] with different physical plant densities (ρ_E) [kg/m^3]: 100 (solid line), 400 (dashed line), 800 (dashed dotted line) on top of a bivariate (2-D) histogram of global, SMAP-derived $\beta_{\text{SMAP}}^{v-vv}$-values (excluding ice-covered regions); coloring of histogram from dark blue (low counts) to yellow (high counts).

(VWC dependence) and magnitude of the $\beta_{\text{Veg}}^{p-pp}$ parameters in the physical covariation model and those estimated from SMAP observations using time-series regression are comparable.

However, the degree to which the covariation model matches with the SMAP observations is different for each polarization. $\beta_{\text{Veg}}^{h-hh}$ envelopes $\beta_{\text{SMAP}}^{h-hh}$ in Fig. 9, whereas $\beta_{\text{Veg}}^{v-vv}$ shows an offset compared to $\beta_{\text{SMAP}}^{v-vv}$ in Fig. 10. The reason is rooted in the nominal parameter settings modeling only three specific, out of all possible natural scenarios.

When modeling both covariations ($\beta_{\text{Veg}}^{h-hh}$, $\beta_{\text{Veg}}^{v-vv}$), the nominal and mainly vertical orientation of the vegetation (see Section III, including Fig. 2 with settings in Table II), leads to vertical covariations $\beta_{\text{Veg}}^{v-vv}$ only partially representing the orientation of vegetation cover on global scales. As shown in Fig. 2, the principal orientation of the lossy dielectric elements in the vegetation layer can modulate the relative magnitudes of the covariation parameter at different polarizations. Moreover, the applied modeling approach of [51], using one homogeneously filled layer of discs above a single-scattering nonpenetrable soil surface is a significant simplification for global variation in vegetation and soil scattering. However, optimization and adaptation of the forward model settings for different landscape conditions are beyond the scope of this paper that focuses on theoretical foundations of a physical forward model for covariation.

IV. Summary and Conclusion

Soil moisture information at high spatial resolution and with global coverage can be obtained with combined use of active and passive microwave remote sensing. Whether it is with measurements from the same platform, such as with the NASA SMAP mission L-band sensors (albeit for short duration) or with combination of microwave radiometers and SAR on different platforms, the physics underlying covariations of active and passive microwaves need to be understood. Relatively, the radiometer measurements are more sensitive to surface soil moisture, but allow only coarse resolution mapping. SAR measurements are more sensitive to surface roughness and vegetation conditions, but have the resolution advantage over radiometer measurements. The optimal mapping capability is built on combining these two measurements through their covariation and taking advantage of the relative strength of each observation. The active and passive microwave measurements are linked through a critical covariation parameter β that can be currently statistically estimated over short (subseasonal) time periods. This parameter is intended to capture the covariations of the active and passive measurements due to changing soil moisture conditions but for given (local) vegetation cover and roughness conditions. The parameter is therefore a function of the characteristics of the vegetation canopy (structure, density, and dielectric constant properties) and their changes over time.

In this paper, we introduce a physics-based forward model for covariation (β) in order to gain insight into how covariation depends on the dominant surface roughness and vegetation conditions. The physical model in case of bare soils ($\beta_{\text{Bare}}^{p-pp}$) is related to surface roughness characteristics such as wavelength-scaled vertical (root-mean-squared height ks) and horizontal (autocorrelation length kl) roughness. Over surfaces with vegetation cover, the physical model ($\beta_{\text{Veg}}^{p-pp}$) is additionally dependent on vegetation structure and orientation, density, and dielectric properties. The forward model incorporates incidence angle dependence which is advantageous with SAR applications. Upon appropriate modification necessary for shifts in measurements frequency, the forward model may be applied to other mixtures of active and passive microwave channels.

The first insight resulting from this paper is that the statistically determined covariation parameter β_{p-pp} is equivalent to the ratio of losses for emission over scattering and losses for backscattering due to surface roughness and vegetation conditions. Hence, these losses and scattering are in turn physically related to surface roughness and vegetation characteristics. The study provides sensitivity analyses with respect to these bio- and pedo-physical parameters. Generally, the covariation, expressed by $\beta_{\text{Bare}}^{p-pp}$ increases toward less-negative values for increasing soil roughness due to the higher roughness-sensitivity of backscatter in comparison with emissivity. Increasing vegetation cover similarly leads to a decrease of covariation magnitudes for $\beta_{\text{Veg}}^{p-pp}$. With the physics-based forward model, the functional dependence on these characterizations of the soil surface and vegetation canopy can now be explored. The proposed forward model for backscatter includes attenuated surface as well as double-bounce terms. The double-bounce term is often the dominant loss contribution at L-band. This effect is more pronounced for denser and thicker plant constituents. For VWC values >5 [kg/m^2] both $\beta_{\text{Veg}}^{h-hh}$ and $\beta_{\text{Veg}}^{v-vv}$ converge to values close to zero, implying a weak, polarization-independent covariation of SAR, and radiometer measurements. Below 5 [kg/m^2] a clear polarization dependence on covariation is evident for vegetated surfaces due to vegetation orientation effects. Vertically polarized $\beta_{\text{Veg}}^{v-vv}$ is closer to zero than horizontally polarized $\beta_{\text{Veg}}^{h-hh}$ if the vegetation is mainly vertically oriented. However, this dependence can be reversed for horizontally oriented vegetated surfaces.

The physical model for covariation is limited to the range of validity of its constituent ingredients. For example the assumption of a single-layer vegetation volume above an impenetrable (no soil volume scattering) soil surface as well as the choice of the physical emission and scattering models used for describing the soil and vegetation interactions limit the range of validity.

In the future and in general, the polarization dependence of vegetation attenuation and scattering need to be incorporated into the $\tau - \omega$ model for passive microwave remote sensing. Modeling and observation-based estimates of polarization-dependent parameters remain a challenge. The physical model for active and passive covariation introduced in this paper is modular and can incorporate improvements in the $\tau - \omega$ model when they are available. Similarly, the characterization of the vegetation topology, distribution, and dielectric properties affects the active microwave measurements. The improvements in the characterization are alternative vegetation models which can be incorporated into the modular model introduced in this paper. Finally, the full range of soil surface roughness cannot be completely captured by the Bragg and Fresnel scattering models. But these constituent model elements can be replaced when applied to very rough surfaces such as ploughed fields.

This paper of the physical forward model of covariation opens the path for follow-on development of physics-based inversion and retrieval algorithms. It also paves the way to explore the expected shifts in the behavior of the covariation parameter when different microwave frequency channels are

used for the emission and backscatter. These extensions are subjects for follow-on studies.

APPENDIX
POLARIZABILITY OF THE VEGETATION BOUNCE

The discrete model of Lang and Sidu [51] describes backscattering from a layer of vegetation over a flat lossy ground using the distorted born approximation. The vegetation layer is composed of lossy dielectric discs with given orientation statistics. Interaction with these discs (vegetation bounce) occurs within combined soil-vegetation (double-bounce) scattering (see Section II-B). The polarizabilities of the vegetation bounce for the double-bounce term for both co-polarizations are [51]

$$\overline{|\alpha_{HH}|^2} = |\overline{\alpha}_{yy}|^2 = |\alpha_r \overline{\sin^2\theta} + \alpha_\theta \overline{\cos^2\theta} + \alpha_\phi|^2 \quad \text{(A.1)}$$

$$\overline{|\alpha_{VV}|^2} = |(-\cos^2\theta_i(\alpha_r \overline{\sin^2\theta} + \alpha_\theta \overline{\cos^2\theta} + \alpha_\phi) + \sin^2\theta_i(\alpha_\theta \overline{\sin^2\theta} + \alpha_r \overline{\cos^2\theta}))|^2. \quad \text{(A.2)}$$

The overbar represents the angular averaging with respect to a distribution of orientation angles θ to a mean orientation angle Θ. A uniform probability density function with orientation range parameter width Δ is used [51]. Orientation θ represents the angle between the z-axis and the normal of the spheroidal particles. Parameters α_r, α_θ, and α_ϕ are a function of the complex dielectric constant of the vegetation ε_V [57]

$$\alpha_r = \frac{\varepsilon_V - 1}{\varepsilon_V} \quad \text{and } \alpha_\theta = \alpha_\phi = \varepsilon_V - 1. \quad \text{(A.3)}$$

ACKNOWLEDGMENT

The authors would like to thank the German Helmholtz Association, Berlin, Germany, and NASA, Washington, DC, USA, for support of the activities. They would also like to thank Dr. L. Tsang and colleagues from the University of Michigan, Ann Arbor, MI, USA, for provision of the NMM3D data for bare soil scattering and emission. In addition, the authors acknowledge MIT support for this research through the MIT-Germany Seed Fund "Global Water Cycle and Environmental Monitoring using Active and Passive Satellite-based Microwave Instruments". Moreover, Prof. P. Ferrazzoli and the anonymous reviewers are greatly acknowledged for their perceptive comments and valuable recommendations.

REFERENCES

[1] L. Gu *et al.*, "Direct and indirect effects of atmospheric conditions and soil moisture on surface energy partitioning revealed by a prolonged drought at a temperate forest site," *J. Geophys. Res. Atmos.*, vol. 111, no. D16, pp. 1–13, 2006.

[2] R. D. Koster *et al.*, "Regions of strong coupling between soil moisture and precipitation," *Science*, vol. 305, no. 5687, pp. 1138–1140, 2004.

[3] K. A. McColl, S. H. Alemohammad, R. Akbar, A. G. Konings, S. Yueh, and D. Entekhabi, "The global distribution and dynamics of surface soil moisture," *Nature Geosci.*, vol. 10, pp. 100–104, Jan. 2017.

[4] S. R. Cloude, *Polarisation: Applications in Remote Sensing*. Oxford, U.K.: Oxford Univ. Press, 2010.

[5] F. T. Ulaby, R. K. Moore, and A. K. Fung, *Microwave and Remote Sensing: Active and Passive: Radar Remote Sensing and Surface Scattering and Emission Theory*, vol. 2. Boston, MA, USA: Artech House, 1982.

[6] J. C. Curlander and R. N. McDonough, *Synthetic Aperture Radar: Systems and Signal Processing*. New York, NY, USA: Wiley, 1991.

[7] F. T. Ulaby, F. K. Moore, and A. K. Fung, *Microwave Remote Sensing: Active and Passive: From Theory to Applications*, vol. 3. Norwood, MA, USA: Artech House, 1986.

[8] N. N. Das, D. Entekhabi, and E. G. Njoku, "An algorithm for merging SMAP radiometer and radar data for high-resolution soil-moisture retrieval," *IEEE Trans. Geosci. Remote Sens.*, vol. 49, no. 5, pp. 1504–1512, May 2011.

[9] D. Entekhabi *et al.*, "The Soil Moisture Active Passive (SMAP) Mission," *Proc. IEEE*, vol. 98, no. 5, pp. 704–716, May 2010.

[10] S. Huang, L. Tsang, E. G. Njoku, and K. S. Chan, "Backscattering coefficients, coherent reflectivities, and emissivities of randomly rough soil surfaces at L-band for SMAP applications based on numerical solutions of Maxwell equations in three-dimensional simulations," *IEEE Trans. Geosci. Remote Sens.*, vol. 48, no. 6, pp. 2557–2568, Jun. 2010.

[11] S. Huang and L. Tsang, "Electromagnetic scattering of randomly rough soil surfaces based on numerical solutions of Maxwell equations in three-dimensional simulations using a hybrid UV/PBTG/SMCG method," *IEEE Trans. Geosci. Remote Sens.*, vol. 50, no. 10, pp. 4025–4035, Oct. 2012.

[12] J. A. Kong, L. Tsang, M. Zuniga, R. Shin, J. C. Shiue, and A. T. C. Chang, "Theoretical modelling and experimental data matching for active and passive microwave remote sensing of earth terrain," in *Proc. Symp. Terrain Profiles Contours EM Wave Propag., AGARD, NATO Meeting*, Norway, 1979, pp. 10–32.

[13] L. Tsang, A. J. Blanchard, R. W. Newton, and J. Au Kong, "A simple relation between Active and passive microwave remote sensing measurements of earth terrain," *IEEE Trans. Geosci. Remote Sens.*, vol. GRS-20, no. 4, pp. 482–485, Oct. 1982.

[14] L. Zhou, L. Tsang, V. Jandhyala, Q. Li, and C. H. Chan, "Emissivity simulations in passive microwave remote sensing with 3-D numerical solutions of Maxwell equations," *IEEE Trans. Geosci. Remote Sens.*, vol. 42, no. 8, pp. 1739–1748, Aug. 2004.

[15] N. S. Chauhan, "Soil moisture estimation under a vegetation cover: Combined active passive microwave remote sensing approach," *Int. J. Remote Sens.*, vol. 18, no. 5, pp. 1079–1097, 1997.

[16] L. Dente, P. Ferrazzoli, Z. Su, R. van de Velde, and L. Guerriero, "Combined use of active and passive microwave satellite data to constrain a discrete scattering model," *Remote Sens. Environ.*, vol. 155, pp. 222–238, Dec. 2014.

[17] Y. Du, F. T. Ulaby, and M. C. Dobson, "Sensitivity to soil moisture by active and passive microwave sensors," *IEEE Trans. Geosci. Remote Sens.*, vol. 38, no. 1, pp. 105–114, Jan. 2000.

[18] P. Ferrazzoli, G. Luzi, S. Paloscia, P. Pampaloni, G. Schiavon, and D. Solimini, "Comarison between the microwave emissivity and backscatter coefficient of crops," *IEEE Trans. Geosci. Remote Sens.*, vol. GRS-27, no. 6, pp. 772–778, Nov. 1989.

[19] P. Ferrazzoli and L. Guerriero, "Synergy of active and passive signatures to decouple soil and vegetation effects," in *Proc. 11th Spec. Meeting Microw. Radiometry Remote Sens. Environ.*, Washington, DC, USA, Mar. 2010, pp. 86–89.

[20] L. Guerriero, P. Ferrazzoli, C. Vittucci, R. Rahmoune, M. Aurizzi, and A. Mattioni, "L-band passive and active signatures of vegetated soil: Simulations with a unified model," *IEEE J. Sel. Topics Appl. Earth Observ. Remote Sens.*, vol. 9, no. 6, pp. 2520–2531, Jun. 2016.

[21] V. K. Gupta, N. Sharma, and R. A. Jangid, "Emission and scattering behaviour of bare and vegetative soil surfaces of different moist states by microwave remote sensing," *Indian J. Radio Space Phys.*, vol. 42, pp. 42–51, Feb. 2013.

[22] P. E. O'Neill, N. S. Chauhan, and T. J. Jackson, "Use of active and passive microwave remote sensing for soil moisture estimation through corn," *Int. J. Remote Sens.*, vol. 17, no. 10, pp. 1851–1865, 1996.

[23] S. S. Saatchi, D. M. Le Vine, and R. H. Lang, "Microwave backscattering and emission model for grass canopies," *IEEE Trans. Geosci. Remote Sens.*, vol. 32, no. 1, pp. 177–186, Jan. 1994.

[24] L. Tsang *et al.*, "Active and passive vegetated surface models with rough surface boundary conditions from NMM3D," *IEEE Trans. Geosci. Remote Sens.*, vol. 6, no. 3, pp. 1698–1709, Jun. 2013.

[25] D. Entekhabi *et al.*, "SMAP handbook," Jet Propuls. Lab., Pasadena, CA, USA, JPL Rep. 400-1567, 2014, pp. 1–192. [Online]. Available: http://smap.jpl.nasa.gov/mission/description/

[26] J. R. Piepmeier *et al.*, "SMAP L-band microwave radiometer: Instrument design and first year on orbit," *IEEE Trans. Geosci. Remote Sens.*, vol. 55, no. 4, pp. 1954–1966, Apr. 2017.

[27] X. Zhan, P. R. Houser, J. P. Walker, and W. T. Crow, "A method for retrieving high-resolution surface soil moisture from hydros L-band radiometer and radar observations," *IEEE Trans. Geosci. Remote Sens.*, vol. 44, no. 6, pp. 1534–1544, Jun. 2006.

[28] S. C. Dunne, D. Entekhabi, and E. G. Njoku, "Impact of multiresolution active and passive microwave measurements on soil moisture estimation using the ensemble Kalman smoother," *IEEE Trans. Geosci. Remote Sens.*, vol. 45, no. 4, pp. 1016–1028, Apr. 2007.

[29] U. Narayan, V. Lakshmi, and E. G. Njoku, "Retrieval of soil moisture from passive and active L/S band sensor (PALS) observations during the soil moisture experiment in 2002 (SMEX02)," *Remote Sens. Environ.*, vol. 92, no. 4, pp. 483–496, 2004.

[30] M. Piles, D. Entekhabi, and A. Camps, "A change detection algorithm for retrieving high-resolution soil moisture from SMAP radar and radiometer observations," *IEEE Trans. Geosci. Remote Sens.*, vol. 47, no. 12, pp. 4125–4131, Dec. 2009.

[31] N. N. Das, D. Entekhabi, E. G. Njoku, J. J. C. Shi, J. T. Johnson, and A. Colliander, "Tests of the SMAP combined radar and radiometer algorithm using airborne field campaign observations and simulated data," *IEEE Trans. Geosci. Remote Sens.*, vol. 52, no. 4, pp. 2018–2028, Apr. 2014.

[32] C. Montzka *et al.*, "Investigation of SMAP fusion algorithms with airborne active and passive L-band microwave remote sensing," *IEEE Trans. Geosci. Remote Sens.*, vol. 54, no. 7, pp. 3878–3889, Jul. 2016.

[33] X. Wu, J. P. Walker, N. N. Das, R. Panciera, and C. Rüdiger, "Evaluation of the SMAP brightness temperature downscaling algorithm using active–passive microwave observations," *Remote Sens. Environ.*, vol. 155, pp. 210–221, Dec. 2014.

[34] X. Wu, J. P. Walker, C. Rüdiger, and R. Panciera, "Effect of land-cover type on the SMAP active/passive soil moisture downscaling algorithm performance," *IEEE Geosci. Remote Sens. Lett.*, vol. 12, no. 4, pp. 846–850, Apr. 2015.

[35] E. G. Njoku *et al.*, "Observations of soil moisture using a passive and active low-frequency microwave airborne sensor during SGP99," *IEEE Trans. Geosci. Remote Sens.*, vol. 40, no. 12, pp. 2659–2673, Dec. 2002.

[36] D. Entekhabi, N. N. Das, E. G. Njoku, J. Johnson, and J. Shi, "Soil Moisture Active Passive: Algorithm theoretical basis document L2 & L3 radar/radiometer Soil Moisture (Active/Passive) data products," Jet Propuls. Lab., Pasadena, CA, USA, JPL Rep., 2012. [Online]. Available: https://smap.jpl.nasa.gov/system/internal_resources/details/original/277_L2_3_SM_AP_RevA_web.pdf

[37] D. J. Leroux *et al.*, "Active–Passive disaggregation of brightness temperatures during the SMAPVEX12 campaign," *IEEE Trans. Geosci. Remote Sens.*, vol. 54, no. 12, pp. 6859–6867, Dec. 2016.

[38] M. Piles, K. A. McColl, D. Entekhabi, N. Das, and M. Pablos, "Sensitivity of aquarius active and passive measurements temporal covariability to land surface characteristics," *IEEE Trans. Geosci. Remote Sens.*, vol. 53, no. 8, pp. 4700–4711, Aug. 2015.

[39] A. Colliander *et al.*, "Comparison of airborne passive and active L-band system (PALS) brightness temperature measurements to SMOS observations during the SMAP validation experiment 2012 (SMAPVEX12)," *IEEE Geosci. Remote Sens. Lett.*, vol. 12, no. 4, pp. 801–805, Apr. 2015.

[40] H. McNairn *et al.*, "The soil moisture active passive validation experiment 2012 (SMAPVEX12): Prelaunch calibration and validation of the SMAP soil moisture algorithms," *IEEE Trans. Geosci. Remote Sens.*, vol. 53, no. 5, pp. 2784–2801, May 2015.

[41] W. Peake, "Interaction of electromagnetic waves with some natural surfaces," *IRE Trans. Antennas Propag.*, vol. 7, no. 5, pp. S324–S329, Dec. 1959.

[42] F. T. Ulaby *et al.*, *Microwave Radar and Radiometric Remote Sensing*. Ann Arbor, MI, USA: Univ. Michigan Press, 2014.

[43] N. S. Chauhan, D. M. Le Vine, and R. H. Lang, "Discrete scatter model for microwave radar and radiometer response to corn: Comparison of theory and data," *IEEE Trans. Geosci. Remote Sens.*, vol. 32, no. 2, pp. 416–426, Mar. 1994.

[44] D. M. L. Vine and M. A. Karam, "Dependence of attenuation in a vegetation canopy on frequency and plant water content," *IEEE Trans. Geosci. Remote Sens.*, vol. 34, no. 5, pp. 1090–1096, Sep. 1996.

[45] L. Tsang, J. A. Kong, and R. T. Shin, *Theory of Microwave Remote Sensing*. New York, NY, USA: Wiley, 1985.

[46] R. Bianchi, M. Davidson, I. Hajnsek, M. Wooding, and C. Wloczyk, "AgriSAR 2006—Final report," Eur. Space Agency, Nordwijik, The Netherlands, Tech. Rep. 19974/06/I-LG, 2006, pp. 1–259.

[47] P. Marzahn and R. Ludwig, "On the derivation of soil surface roughness from multi parametric PolSAR data and its potential for hydrological modeling," *Hydrol. Earth Syst. Sci.*, vol. 13, pp. 381–394, Mar. 2009.

[48] Q. Li, J. Shi, and K. S. Chen, "A generalized power law spectrum and its applications to the backscattering of soil surfaces based on the integral equation model," *IEEE Trans. Geosci. Remote Sens.*, vol. 40, no. 2, pp. 271–280, Feb. 2002.

[49] M. Born and E. Wolf, *Principles of Optics: Electromagnetic Theory of Propagation, Interference and Diffraction of Light*. Cambridge, U.K.: Cambridge Univ. Press, 1999.

[50] M. C. Dobson and F. T. Ulaby, "Preliminaly evaluation of the SIR-B response to soil moisture, surface roughness, and crop canopy cover," *IEEE Trans. Geosci. Remote Sens.*, vol. GRS-24, no. 4, pp. 517–526, Jul. 1986.

[51] R. H. Lang and J. S. Sidhu, "Electromagnetic backscattering from a layer of vegetation: A discrete approach," *IEEE Trans. Geosci. Remote Sens.*, vol. GRS-21, no. 1, pp. 62–71, Jan. 1983.

[52] L. Tsang, J. A. Kong, and K.-H. Ding, *Scattering of Electromagnetic Waves: Theories and Applications*. New York, NY, USA: Wiley, 2000.

[53] E. P. W. Attema and F. T. Ulaby, "Vegetation modeled as a water cloud," *Radio Sci.*, vol. 13, no. 2, pp. 357–364, Mar./Apr. 1978.

[54] H. J. Eom and A. K. Fung, "A scatter model for vegetation up to Ku-band," *Remote Sens. Environ.*, vol. 15, no. 3, pp. 185–200, 1984.

[55] L.-J. Du and W. H. Peake, "Rayleigh scattering from leaves," *Proc. IEEE*, vol. 57, no. 6, pp. 1227–1229, Jun. 1969.

[56] M. A. Karam and A. K. Fung, "Scattering from randomly oriented circular discs with application to vegetation," *Radio Sci.*, vol. 18, no. 4, pp. 557–565, Jul./Aug. 1983.

[57] R. H. Lang, "Electromagnetic backscattering from a sparse distribution of lossy dielectric scatterers," *Radio Sci.*, vol. 16, no. 1, pp. 15–30, 1981.

[58] T. J. Jackson and T. J. Schmugge, "Vegetation effects on the microwave emission of soils," *Remote Sens. Environ.*, vol. 36, no. 3, pp. 203–212, Jun. 1991.

[59] P. O'Neill, S. Chan, E. Njoku, T. Jackson, and R. Bindlish, "Algorithm theoretical basis document level 2 & 3 Soil Moisture (Passive) data products," Jet Propuls. Lab., Pasadena, CA, USA, SMAP Project, JPL D-66480, 2014.

[60] J.-P. Wigneron *et al.*, "Modelling the passive microwave signature from land surfaces: A review of recent results and application to the L-band SMOS & SMAP soil moisture retrieval algorithms," *Remote Sens. Environ.*, vol. 192, pp. 238–262, Apr. 2017.

[61] A. G. Konings, M. Piles, K. Rötzer, K. A. McColl, S. K. Chan, and D. Entekhabi, "Vegetation optical depth and scattering albedo retrieval using time series of dual-polarized L-band radiometer observations," *Remote Sens. Environ.*, vol. 172, pp. 178–189, Jan. 2016.

[62] J.-P. Wigneron, J.-C. Calvet, A. Chanzy, O. Grosjean, and L. Laguerre, "A composite discrete-continuous approach to model the microwave emission of vegetation," *IEEE Trans. Geosci. Remote Sens.*, vol. 33, no. 1, pp. 201–211, Jan. 1995.

[63] T. Jagdhuber, I. Hajnsek, and K. P. Papathanassiou, "An iterative generalized hybrid decomposition for soil moisture retrieval under vegetation cover using fully polarimetric SAR," *IEEE J. Sel. Topics Appl. Earth Observ. Remote Sens.*, vol. 8, no. 8, pp. 3911–3922, Aug. 2015.

[64] A. K. Fung and K.-S. Chen, *Microwave Scattering and Emission Models for Users*. Norwood, MA, USA: Artech House, 2010.

[65] W. H. Peake, "Interaction of electromagnetic waves with some natural surfaces," Ph.D. dissertation, Dept. Phys. Astron., Ohio State Univ., Columbus, OH, USA, 1959.

[66] A. A. Chukhlantsev, "Microwave radiometry of vegetation canopies," in *Advances in Global Change Research*, vol. 24, M. Beniston, Ed. Amsterdam, The Netherlands: Springer, 2006.

[67] Y. Kim, T. J. Jackson, R. Bindlish, K. Lee, and S. Hong, "Radar vegetation index for estimating the vegetation water content of rice and soybean," *IEEE Geosci. Remote Sens. Lett.*, vol. 9, no. 4, pp. 564–568, Jul. 2012.

[68] Y. Kim and J. van Zyl, "Vegetation effects on soil moisture estimation," in *Proc. IEEE Geosci. Remote Sens. Symp.*, Anchorage, AK, USA, Sep. 2004, pp. 800–802.

[69] J. S. Lee and E. Pottier, *Polarimetric Radar Imaging: From Basics to Applications*. Boca Raton, FL, USA: CRC Press, 2009.

[70] T. Jagdhuber and I. Hajnsek, "Model-based inversion of soil parameters under vegetation using ground-to-volume ratios," in *Proc. 8th Eur. Conf. Synth. Aperture Radar (EUSAR)*, Aachen, Germany, Jun. 2010, pp. 495–498.

[71] T. Jagdhuber, "Soil parameter retrieval under vegetation cover using SAR polarimetry," Ph.D. dissertation, Univ. Potsdam, Potsdam, Germany, 2012. [Online]. Available: http://nbn-resolving.de/urn:nbn:de:kobv:517-opus-60519

[72] D. Entekhabi, N. Das, E. G. Njoku, J. T. Johnson, and J. Shi, "SMAP L2 radar/radiometer half-orbit 9 km EASE-grid soil moisture, version 3. [Global]," NASA Nat. Snow Ice Data Center Distrib. Act. Arch. Center, Boulder, CO, USA, 2016. [Online]. Available: https://nsidc.org/data/spl2smap, doi: 10.5067/.8YTYSV6JGBK2.

Thomas Jagdhuber (S'08–M'12) received the Diploma degree (Hons.) in physical geography, physics, remote sensing and geoinformatics from the Ludwig Maximilian University of Munich, Munich, Germany, in 2006, and the Ph.D. degree (Hons.) in hydrology from the Faculty of Science, University of Potsdam, Potsdam, Germany, in 2012.

Since 2007, he has been with the Microwaves and Radar Institute (HR), German Aerospace Center (DLR), Oberpfaffenhofen, Germany. From 2014 to 2018, he was a yearly Visiting Scientist at the Massachusetts Institute of Technology (MIT), Boston, MA, USA, contributing to the preparation and continuation of the SMAP and SMAP/Sentinel-1 missions. He serves as a Lecturer for the University of Jena, Jena, Germany, and the University of Augsburg, Augsburg, Germany. His research interests include physics-based multisensor data integration with a focus on active and passive microwave interaction theory and on polarimetric techniques for hydrological, cryospheric, and agricultural parameter modeling and estimation.

Dr. Jagdhuber was honored with the DLR Science Award for his research on polarimetric SAR decomposition techniques in 2014. Together with Prof. Dr. Entekhabi, MIT, he was awarded with the MIT-MISTI grant for global water cycle and environmental monitoring using active and passive satellite-based microwave instruments. He serves as a reviewer for several international journals and conference boards.

Alexandra G. Konings (S'12–M'16) received the B.S. degree in environmental engineering from the Massachusetts Institute of Technology (MIT), Cambridge, MA, USA, in 2009, the M.S. degree in environmental science from Duke University, Durham, NC, USA, in 2011, and the Ph.D. degree in environmental engineering from MIT in 2015.

From 2015 to 2016, she was a Visiting Post-Doctoral Associate with the Department of Earth and Environmental Engineering, Columbia University, New York, NY, USA, and with the Carbon Cycle and Ecosystems Group, NASA Jet Propulsion Laboratory, Pasadena, CA, USA. She is currently an Assistant Professor with the Department of Earth System Science, Stanford University, Stanford, CA, USA. Her research interests include studies of coupling between the water and carbon cycles, ecohydrology, and active and passive microwave remote sensing of soil moisture and vegetation water content.

Dr. Konings received the NASA New (Early Career) Investigator Award in 2017.

Kaighin A. McColl (S'09–M'17) received the Bachelor of Environmental Engineering (Hons.) and Bachelor of Science (applied mathematics) degrees from the University of Melbourne, Parkville, VIC, Australia, and the Ph.D. degree from the Massachusetts Institute of Technology (MIT), Cambridge, MA, USA, in 2017.

He was funded by the National Science Foundation's Graduate Research Fellowship Program. He is currently an Assistant Professor with the Department of Earth and Planetary Sciences, and with the Harvard John A. Paulson School of Engineering and Applied Sciences, Harvard University, Cambridge, MA, USA. His research interests include hydrometeorology, boundary-layer meteorology, land–atmosphere interactions, and remote sensing of soil moisture and vegetation.

Seyed Hamed Alemohammad (M'15) received the B.Sc. degree in civil engineering and the M.Sc. degree in water resources from the Sharif University of Technology, Tehran, Iran, in 2007 and 2009, respectively, and the Ph.D. degree in civil and environmental engineering from the Massachusetts Institute of Technology (MIT), Cambridge, MA, USA, in 2015.

He was a Post-Doctoral Research Scientist at Columbia University, New York, NY, USA, from 2016 to 2017, and a Post-Doctoral Research Associate at MIT from 2014 to 2016. He is currently the Lead Geospatial Data Scientist with Radiant.Earth, Washington, DC, USA. His research interests include applications of multispectral and passive/active microwave observations for land surface monitoring, and machine learning techniques applied to large-scale earth observation data.

Narendra Narayan Das was born in Bhilai, India. He received the Bachelor of Engineering degree from the National Institute of Technology, Raipur, India, and the Master and Ph.D. degrees from Texas A&M University, College Station, TX, USA, in 2005 and 2008, respectively.

In 2008, he joined the Jet Propulsion Laboratory (JPL), Pasadena, CA, USA, and has been conducting research in hydrology and microwave remote sensing research on land. He is currently a Research Scientist with the Surface Hydrology Group, Climate, Oceans, and Solid Earth Science Section, JPL. He is also a Key Member of the Science Algorithm Development Team for the Soil Moisture Active and Passive mission.

Carsten Montzka (M'17) received the Ph.D. degree in geography from the University of Bonn, Bonn, Germany, in 2007, with a focus on the integration of multispectral remote sensing data into nitrogen cycle simulations.

In 2004, he joined the Institute of Bio- and Geosciences: Agrosphere (IBG-3) of the Forschungszentrum Jülich, Jülich, Germany. Since 2007, he has been focused on passive microwave retrieval for soil moisture and SMOS and SMAP validation activities. This includes modeling and upscaling of surface soil moisture, coupling hydrological models with microwave emission models, multiscale model calibration, and comparison with and integration of airborne remote sensing data. Recently, he has been selected for the Arab-German Young Academy for Sciences and Humanities, Berlin, Germany. His research interests include the development of multiscale soil moisture data assimilation techniques and airborne active/passive microwave campaigns to support the SMAP mission.

Moritz Link (S'17) received the B.S. degree in physical geography and the M.S. degree in environmental systems and sustainability from the Ludwig-Maximilian University of Munich, Munich, Germany, in 2014 and 2017, respectively.

In 2014 and from 2015 to 2017, he was with the Microwaves and Radar Institute, German Aerospace Center (DLR), Oberpfaffenhofen, Germany. From 2016 and 2017, he was visiting the Department of Civil and Environmental Engineering, Massachusetts Institute of Technology, Cambridge, MA, USA. He is currently conducting research at the European Space Research and Technology Center, European Space Agency, Noordwijk, The Netherlands. His research interests include active and passive microwave remote sensing of soil moisture and other land surface variables.

Ruzbeh Akbar (S'05–M'13) received the B.S. degree (*summa cum laude*) in electrical engineering from The George Washington University, Washington, DC, USA, in 2009, the M.S. degree in electrical engineering from the University of Michigan, Ann Arbor, MI, USA, in 2011, and the Ph.D. degree in electrical engineering from the University of Southern California, Los Angeles, CA, USA, in 2016.

He is currently a Post-Doctoral Research Associate with the Massachusetts Institute of Technology, Cambridge, MA, USA. His research interests include terrestrial remote sensing, electromagnetic theory, and hydrology.

Dr. Akbar was a recipient of the NASA Earth and Space Science Fellowship from 2010 to 2014.

Dara Entekhabi (M'04–SM'09–F'15) received the B.S. and M.S. degrees in geography from Clark University, Worcester, MA, USA, in 1983 and 1988, respectively, and the Ph.D. degree in civil and environmental engineering from the Massachusetts Institute of Technology (MIT), Cambridge, MA, USA, in 1990.

He is currently a Professor with the Department of Civil and Environmental Engineering and also with the Department of Earth, Atmospheric and Planetary Sciences, MIT. He is the Science Team Lead of the National Aeronautics and Space Administration's Soil Moisture Active and Passive mission that was launched in 2015. His research interests include terrestrial remote sensing, data assimilation, and coupled land–atmosphere systems modeling.

Dr. Entekhabi is also a fellow of the American Meteorological Society and the American Geophysical Union. He is a member of the National Academy of Engineering.